Combined H_∞-Feedback Control and Iterative Learning Control Design With Application to Nanopositioning Systems

Brian E. Helfrich, Chibum Lee, *Student Member, IEEE*, Douglas A. Bristow, X. H. Xiao, Jingyan Dong, A. G. Alleyne, Srinivasa M Salapaka, *Member, IEEE*, and Placid M. Ferreira

***Abstract*—This paper examines a coordinated feedback and feedforward control design strategy for precision motion control (PMC) systems. It is assumed that the primary exogenous signals are repeated; including disturbances and references. Therefore, an iterative learning control (ILC) feedforward strategy can be used. The introduction of additional non-repeating exogenous signals, including disturbances, noise, and reset errors, necessitates the proper coordination between feedback and feedforward controllers to achieve high performance. A novel ratio of repeated versus non-repeated signal power in the frequency domain is introduced and defined as the repetitive-to-non-repetitive (RNR) ratio. This frequency specific ratio allows for a new approach to delegating feedback and feedforward control efforts based on RNR value. A systematic procedure for control design is given whereby the feedback addresses the non-repeating exogenous signal content ($\mathrm{RNR} < 0\ \mathrm{dB}$) and the feedforward ILC addresses the repeating signal content ($\mathrm{RNR} > 0\ \mathrm{dB}$). To illustrate the design approach, two case studies using different nano-positioning devices are given.**

***Index Terms*—Iterative learning control (ILC), nanopositioning, precision motion control (PMC).**

I. Introduction

TECHNOLOGICAL advancements in high precision manufacturing processes have produced a need for increased research in precision motion control (PMC) [1], [2] techniques. PMC systems can utilize feedback or feedforward control designs or a combination of both feedforward and feedback in a two-degree-of-freedom approach. Effective feedback design tools for nanopositioning include H_∞ robust [3], [4], state feedback [5], and double-integrator derivative [6] control to name a few. Additionally, for systems that repeat the same trajectory, as in the case of many manufacturing processes, iterative learning control (ILC) [7]–[10] is a good choice for feedforward control design. The goal of this article is to present a frequency-based design methodology to improve the overall system performance by delegating the roles of feedback and ILC controllers based on known classes of exogenous signals.

This investigation is motivated by physical phenomena. The class of physical systems under consideration consists of a structure, possibly multi-degree-of-freedom, which is forced by some type of actuation device. These could be small flexure-based structures with piezo actuators, as with atomic force microscope stages [11], or large inertia masses driven electromagnetically, such as wafer scanning stages [12]. By design, these systems tend to have well defined dynamics in the low frequency range, where "low" is relative to the 1st structural resonance. For the flexure-based systems, the dynamics are essentially a gain; for the inertia systems, the dynamics are essentially a double integrator. Above the first structural resonance, there are usually higher order structural modes that are lightly damped. Additionally, these modes can have very different frequency characteristics at different locations in the flexure stage's work envelope. The high number of structural modes, and the fact that they vary with stage position, makes them difficult to compensate with feedback control. A clear identification of the known dynamics in the frequency domain suggests the use of modern robust control design tools such as H_∞-feedback controllers. These tools are good for point to point regulation and lower frequency tracking.

For higher frequency tracking, it is advantageous to include a feedforward controller in the PMC system. The feedforward controller is usually an approximate inverse of the plant. For trajectories that repeat themselves, a very successful approach is to learn the feedforward signals for subsequent trials by iteratively updating them based on the error accumulated in previous trials. This approach has been formalized as ILC [7]–[10]. ILC has the benefit of not requiring a very accurate plant model yet still giving high performance tracking inputs. While an explicit plant model is not required, it can often be useful in the design of the ILC to minimize the number of iterations taken to converge to an appropriate feedforward input signal.

The primary assumptions for ILC systems include the fact that all exogenous signals, i.e., references and disturbances, are identical from trial to trial. Additionally, current ILC practice assumes that the initial conditions for the system are also identical at the start of each trial. As will be seen by experimental examples, those assumptions are violated in the current work necessitating a modification to current ILC practice. In particular,

Manuscript received July 31, 2008. Manuscript received in final form March 15, 2009. First published July 21, 2009; current version published February 24, 2010. Recommended by Associate Editor S. Devasia. This work was supported by the Nano-CEMMS Center, University of Illinois, which is funded by the NSF under Grant DMI-0328162, and by the MechSE Department fellowship.

A. Alleyne, P. Ferreira, B. Helfrich, C. Lee, S. M. Salapaka, and X. Xiao are with the Department of Mechanical Science and Engineering, University of Illinois, Urbana, IL 61801 USA.

D. Bristow is with the Department of Mechanical and Aerospace, Missouri University of Science and Technology, Rolla, MO 65409 USA.

J. Dong is with the Department of Industrial and Systems Engineering, North Carolina State University, Raleigh, NC 27695 USA.

Color versions of one or more of the figures in this paper are available online at http://ieeexplore.ieee.org.

Digital Object Identifier 10.1109/TCST.2009.2018835

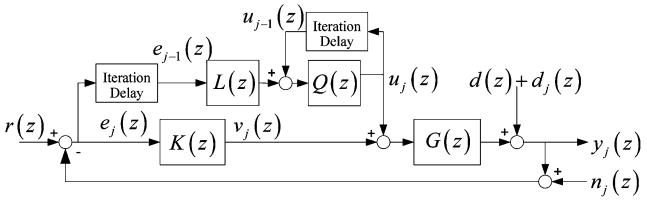

Fig. 1. Block diagram of feedback and ILC system.

this work examines the effect of non-repeating disturbances and imperfect resetting on ILC systems. Previous work [13]–[16] has examined the effects of imperfect resetting on ILC. ILC algorithms can be designed to converge stably to a finite level of error performance depending on the size and nature of the reset error. In contrast, this work has the ILC de-emphasize the reset errors, and any other nonrepetitive signals. The algorithm given here relies on an appropriately co-designed feedback controller to compensate for the nonrepetitive signals. As will be seen, frequency based delegation will be key to mitigating the effects of all exogenous signals on the output error.

In this work, two nanopositioning devices with multiple degrees of freedom are considered in an effort to show the generality of the design approach presented. The actuator layout is different for both systems. Serial kinematics is observed in one of the devices, whereas the other device has parallel kinematics. The serial kinematic device is used as a single input single output (SISO) system for simplifying the design approach presented here. Then, a more complex multiple-input multiple-output (MIMO) system is investigated, which is the parallel kinematic device.

The rest of this paper is organized as follows. Section II gives a brief background for the design of both H_∞-feedback and ILC control schemes. This gives a common platform to describe coordination. Section III introduces an essential component to the controller design procedure, which is the exogenous signal analysis. Key to the coordination of feedback and feedforward algorithms is the knowledge of relative signal power between repeatable and nonrepeatable signals in the frequency spectrum. The overall design strategy employed to coordinate the two controller degrees of freedom is presented in Section IV. The two experimental systems are tested for tracking performance in Section V using the design procedure in Section IV. Concluding remarks are then made in Section VI.

II. Controller Design Background

The PMC system layout used in this work is seen in Fig. 1. The block components in the diagram represent the plant model, $G(z)$, feedback controller, $K(z)$, and the feedforward ILC. Signals identified in the figure include: the reference, $r(z)$, error, $e_j(z)$, noise, $n_j(z)$, output, $y_j(z)$, repeating disturbance, $d(z)$, non-repeating disturbance, $d_j(z)$, learning control, $u_j(z)$, and the feedback control signal, $v_j(z)$. The argument (z) denotes that the analysis was done in discrete time. A subscript "j" represents the iteration for a signal that changes from trial to trial. For example, the iteration delay block takes the error or input at iteration j, (e_j, u_j) and maps it to error and iteration in the subsequent $j-1$ iteration (e_{j-1}, u_{j-1}). For a more detailed explanation, the interested reader is referred to [10]. The system in Fig. 1 will be referred to throughout this work.

General assumptions were made to simplify the design and analysis, which are listed as follows.

A1) All signals are assumed to be infinite in time for frequency domain analysis.

A2) The expected value, or mean, of $n_j(z)$ and $d_j(z)$ is assumed to be zero.

Assumption A1 is used to allow a frequency domain representation of the signals and systems used in this work. Since all practical trajectories are finite, the ILC designs and results given here may be more conservative than possible under a lifted framework. However, the benefit is the ability to utilize frequency domain tools for codesign of feedforward and feedback algorithms.

A. Stand-Alone H_∞-Feedback Control Design

A number of advanced feedback control designs are available [1], but one of the most prevalent strategies used in PMC systems is the H_∞-feedback controller [11], [17]. Design goals for the H_∞-feedback controller include maintaining stability while delivering adequate performance (i.e., bandwidth) and high resolution, i.e., ($d_j(z)$, $d(z)$, and $n_j(z)$ attenuation) under the influence of uncertainties in the operating environment. Classical control design approaches, such as proportional–integral–differential (PID) or lead-lag control, require an ineffective search across the space of controller parameters that meet performance and resolution requirements. An advantage of the H_∞-feedback control design approach is that the specifications set for performance, resolution, and robustness to model uncertainty can be directly considered in the frequency domain via appropriate weighting functions. Then a mathematical optimization framework [18] can be utilized to effectively search for a design.

Common closed-loop transfer functions used for H_∞-feedback control design, $S(z)$, $T(z)$, and $KS(z)$ are defined as

$$S(z) = \frac{y_j(z)}{d_j(z)} = \frac{y_j(z)}{d(z)} = (I + G(z)K(z))^{-1} \quad (1)$$

$$T(z) = \frac{y_j(z)}{r(z)} = (I + G(z)K(z))^{-1} G(z)K(z) \quad (2)$$

$$KS(z) = \frac{v_j(z)}{r(z)} = K(z)(I + G(z)K(z))^{-1}. \quad (3)$$

For a stand-alone H_∞-feedback controller design, we assume $u_j(z) = 0$, and thus, $e_j(z)$ is given by

$$\begin{aligned} e_j(z) &= r(z) - y_j(z) - n_j(z) \\ &= S(z)r(z) - S(z)d(z) - S(z)d_j(z) - T(z)n_j(z). \end{aligned} \quad (4)$$

From (4), we see that a sufficient condition to minimize the error is both $S(z)$ and $T(z)$ should be small. That is, the sensitivity function, $S(z)$, must be small to mitigate the effects of $r(z)$, $d(z)$, and $d_j(z)$. The complimentary sensitivity function, $T(z)$, should be minimized to decrease the presence of $n_j(z)$ in the error signal. It is not possible to design both $S(z)$ and $T(z)$ small for all frequencies due to the relationship

$$S(z) + T(z) = 1. \quad (5)$$

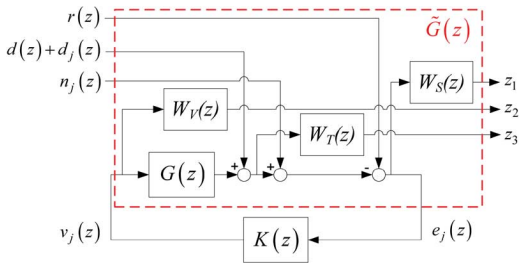

Fig. 2. H_∞ design weighting functions.

This is a key tradeoff in linear feedback controller design, and it stems from the well known Bode's integral [19]–[21] defined as

$$\int_{-\pi}^{\pi} \log |S(z)|\, dz = 0. \tag{6}$$

Thus, if $|S(z)|$ needs to be small at low frequency for small tracking error, this will create large magnitude in $S(z)$ at a different frequency region. The result of increasing $S(z)$ in a specific frequency range is a decrease in the system's closed loop bandwidth, where the bandwidth is defined at the crossover frequency or $|S(z)| = -3$ dB [3]. This phenomenon is known as the "waterbed" effect [3], and it serves to illustrate that there is always a fundamental tradeoff and limitation among bandwidth, robustness, and tracking error.

The controller transfer function, $K(z)$, is obtained through an iterative design of weighting functions to minimize

$$\gamma = \left\| \begin{array}{c} W_S(z)\, S(z) \\ W_T(z)\, T(z) \\ W_V(z)\, KS(z) \end{array} \right\|_\infty \tag{7}$$

where $|X(z)|_\infty = \max_{\omega\in[-\pi,\pi]} \left|X\left(e^{i\omega}\right)\right|$. The weighting functions $\{W_S(z), W_T(z), W_V(z)\}$, which can be seen in Fig. 2, penalize the error, output, and the controller output, respectively; these functions achieve the design objective by shaping the controller. Solutions to this minimization problem are well known [18], and iterative numerical techniques are widely available, e.g., in MATLAB software [22]. In the following, we summarize standard guidelines for the solution of $W_S(z)$, $W_T(z)$, and $W_V(z)$. The interested reader is referred to [3] and [4] for a more detailed discussion.

The transfer function $W_S(z)$ is typically chosen to have high gains at low frequencies and low gains at high frequencies. This scaling ensures that the optimal feedback law is such that $S(z)$ is small at low frequencies, thereby guaranteeing good tracking at the frequencies of interest. The weighting function $W_T(z)$ is often chosen such that it has high gains at high frequencies and low gains at low frequencies. This is done to shape $T(z)$ such that it "rolls off" at high frequencies for noise attenuation. The weighting function for the control $W_V(z)$ is chosen to ensure that the control signals remain within saturation limits. The Bode diagram in Fig. 3 shows general shapes for $W_S(z)$, $W_T(z)$, and $W_V(z)$.

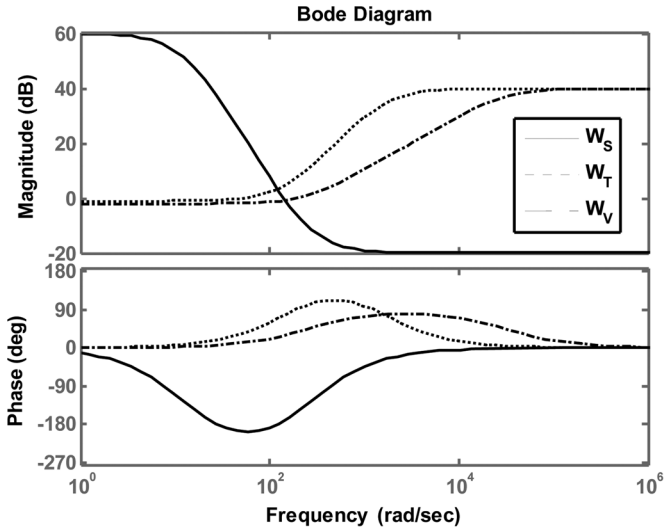

Fig. 3. General shapes for weighting functions.

B. ILC Design

ILC [7]–[10] is used to improve the performance of systems that repeat the same operation many times. ILC uses the tracking errors from previous iterations of the repeated motion to generate a feedforward control signal for subsequent iterations. Convergence of the learning process results in a feedforward control signal that is customized for the repeated motion, yielding very low tracking error. For the purposes of the ILC design, we assume that the feedback controller is given, and therefore $S(z)$ is fixed.

The ILC structure considered in this work is a plant inversion type [10], which is used for fast convergence of the feedforward control signal. In this structure, the error signal is filtered through a learning function $L(z)$ and a Q-filter $Q(z)$. $L(z)$ is a stable inversion of $P(z)$ up to a given frequency, which maps the error signal to the control signal. The use of a plant inversion approach is dependent on an accurate plant model. If such a model does not exist, a PD type learning law may be appropriate. $Q(z)$ is a robustness filter that can be designed to compensate for, among other things, uncertainty in the plant model $P(z)$. Additionally, $Q(z)$ is used to limit the frequency range of the learning for stability and noise attenuation. ILC holds previous control signals in memory and generates a control based on this error stored in memory (8)

$$u_j(z) = Q(z)\left(u_{j-1}(z) + L(z)\, e_{j-1}(z)\right). \tag{8}$$

This control signal is dependent on $e_{j-1}(z)$, which is derived from Fig. 1 and shown as follows:

$$\begin{aligned} e_{j-1}(z) = {} & -G(z)S(z)u_{j-1}(z) + S(z)(r(z) - d(z) - d_{j-1}(z)) \\ & + T(z)n_{j-1}(z). \end{aligned} \tag{9}$$

One of ILC's fundamental limitations is its inability to compensate for non-repeating error or disturbances, $d_j(z)$. This will be demonstrated in the experimental results of this work. The well-known frequency domain ILC stability condition is

$$\left\| Q(z)\left(I - L(z)\, P(z)\right)\right\|_\infty < 1. \tag{10}$$

For fast convergence [10], we select $L(z) = S^{-1}(z)G^{-1}(z)$, which is the ILC plant inversion technique previously mentioned. Note that when $S(z)G(z)$ is strictly proper, $L(z)$ is improper. An improper learning function can be implemented by appropriately shifting the error signal during the learning process [10]. When $S(z)G(z)$ is non-minimum phase, then $L(z)$ is unstable, which can lead to large control signals. In this case, the learning function can be separated into stable and unstable components. Then, these two components are stably filtered in the forward time with the stable component and then in negative time with the unstable component [23]. Other references for stable-inversion for non-minimum phase systems can be found in [24].

Typically, there will be frequencies for which the system model is inaccurate. Equation (10) illustrates that for large uncertainties in some frequency range (e.g., gain uncertainty larger than 100%) we must have $|Q(z)| \ll 1$ in that frequency range for robust stability of the ILC.

The performance of the ILC at convergence is measured by the power spectrum of $e_\infty(z) \triangleq \lim_{j\to\infty} e_j(z)$. In the following the "z" transfer function argument is dropped for compactness. We multiply (8) by *GS*

$$GSu_j = QGSu_{j-1} + QGSLe_{j-1}. \tag{11}$$

Next, substituting (9) for GSu_j and GSu_{j-1} results in

$$\begin{aligned} e_j = {} & Q(1 - GSL)e_{j-1} + (1-Q)S(r-d) \\ & - S(d_j + Qd_{j-1}) + T(n_j - Qn_{j-1}). \end{aligned} \tag{12}$$

Since $L = S^{-1}G^{-1}$, the e_j term conditionally depends on Q as

$$e_j = \begin{cases} -S(d_j - d_{j-1}) + T(n_j - n_{j-1}), & \text{for } Q = 1 \\ S(r-d) - Sd_j + Tn_j, & \text{for } Q = 0 \end{cases}. \tag{13}$$

The interested reader is referred to [25] for further analysis.

The typical Q-filter design is a low pass filter [26]. This is because the system is usually well known at low frequencies, and non-repeating disturbances are minimized by the feedback controller at low frequencies. A tradeoff exists between minimizing repeatable error and amplifying noise when designing the Q-filter. When $Q = 1$, the repeatable error is eliminated, but the noise is amplified. Alternatively, $Q = 0$ has no effect on the noise or repeatable signal. Therefore, we want to vary the value of Q with respect to frequency. We should set $Q = 1$ in frequency regions where the repeatable component, $S(r-d)$, is dominant, and set $Q = 0$ where the nonrepeatable component, $Sd_j + \mathrm{Tn}_j$ is dominant. The Section III will give a detailed procedure on how to determine the repeating and non-repeating content in the error signal $e_j(z)$.

III. Signal Analysis

When tracking repeating reference signals, ILC can be used to mitigate error that is repeated from trial to trial. If non-repeating error enters the learning function, the ILC signal does not converge effectively and can cause an increase in the tracking error. On the other hand, feedback control does not differentiate between repeating or non-repeating error; therefore, we can assign $K(z)$ to reduce non-repeating error and ILC to mitigate the repetitive error. But first, it is imperative that we identify repeating and non-repeating error seen in the PMC system, which is discussed in the following paragraphs.

We need to define the repeating and non-repeating error elements in terms of the components in Fig. 1. The complete error signal has already been determined in (4), so the only requirement is to identify which exogenous signals are repeating or non-repeating. The components appearing in the repeating error would be $r(z)$ and $d(z)$. The non-repeating error would be compiled from $d_j(z)$ and $n_j(z)$. For this analysis, and throughout the remainder of this paper, we assume the noise, $n_j(z)$, occurs at high frequencies and can be eliminated by appropriate filter design. Equations (14) and (15) respectively derive the repeating and non-repeating error in the discrete z-domain and frequency domain

$$\begin{aligned} \bar{e}(z) &\triangleq S(z)(r(z) - d(z)) \to \mathrm{R}(\omega) \\ &= |FFT[\bar{e}(z)]|^2 \end{aligned} \tag{14}$$

$$\begin{aligned} \tilde{e}_j(z) &\triangleq -S(z)d_j(z) \to \mathrm{NR}(\omega) \\ &= \sum_{j=1}^{N} |FFT[\tilde{e}_j(z)]|^2. \end{aligned} \tag{15}$$

A useful measure that can be used to directly compare the $R(\omega)$ to $\mathrm{NR}(\omega)$ signal content is by the repeatable-to-nonrepeatable ratio (RNR) of signal power. The RNR was introduced in [27] and is defined in the following manner (16):

$$\begin{aligned} \mathrm{RNR}(\omega) &\triangleq 20^* \log_{10}\left(\frac{\mathrm{R}(\omega)}{\mathrm{NR}(\omega)}\right) \\ &= 20^* \log_{10}\left(\frac{|FFT[S(z)(r(z) - d(z))]|^2}{\sum_{j=1}^{N} |FFT[S(z)d_j(z)]|^2}\right). \end{aligned} \tag{16}$$

As can be seen from (16), the RNR is scaled in the numerator and denominator by the sensitivity function $S(z)$. $S(z)$ can then be cancelled, so this RNR calculation is not affected by a change in the $S(z)$ or, in other words, not affected by the $K(z)$ design. These theoretical equations work well for analysis, but $d(z)$ and $d_j(z)$ can not be directly measured from an experimental system. We will approximate $\bar{e}(z)$ and $\tilde{e}(z)$ from experimental data in the following manner:

$$\bar{e}(z) \cong \sum_{j=1}^{N} e_j(z) \text{ for } N \gg 1 \tag{17}$$

$$\tilde{e}_j(z) \cong e_j(z) - \bar{e}(z). \tag{18}$$

A standalone feedback controller is used to stabilize the closed-loop system in order to record multiple iterations of tracking error signals. Repetitive error, $\bar{e}(z)$, is found by averaging the tracking error signals in the time domain (17). Non-repeating error, $\tilde{e}(z)$, is approximated by subtracting $\bar{e}(z)$ from each trial's tracking error (18). A conversion of these two signals from the time domain to the frequency domain via the Fast Fourier Transform is performed, because the controller design is based in the frequency domain. Equations (17) and (18)

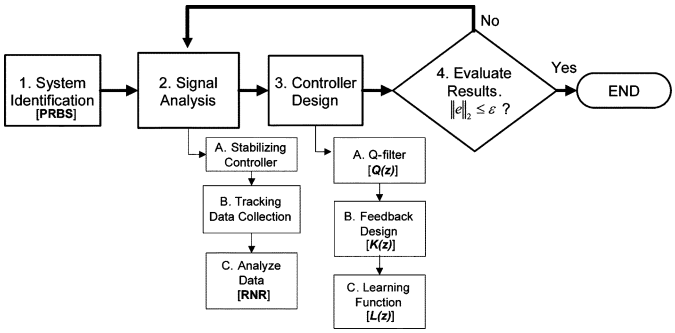

Fig. 4. Combined design method.

are used to calculate the repeating, $R(\omega)$, and non-repeating error, $\mathrm{NR}(\omega)$, respectively.

The RNR is then calculated using (16). This RNR function leads to the design of the combined controller. The design process is discussed in Section IV.

IV. Combined Controller Design

This section presents a heuristic design procedure that utilizes a priori knowledge of the error signal content in the design of the feedback and ILC controllers. A flowchart of the procedure is depicted in Fig. 4. Within the blocks of Fig. 4 are some of the key control elements introduced in Fig. 1.

The first step is the development of a model for the particular system of interest by means of system identification. Two common techniques for system identification are by the use of a swept sine input for frequency domain identification or using a pseudo random binary sequence (PRBS) input to identify the model in the time domain [28]. The former is used in Section V-A and the latter in Section V-B. For both cases, a discrete linear time invariant (LTI) model was estimated using the System Identification Toolbox in MATLAB [29].

Once a model has been identified, a stabilizing controller can be designed to track the desired reference signal. Experimental tracking data for several iterations is collected and then used to differentiate repeating and non-repeating error content. By using the process in Section III, the $R(\omega)$, $\mathrm{NR}(\omega)$, and $\mathrm{RNR}(\omega)$ signals can be estimated.

Frequency regions where $\mathrm{RNR} > 0$ dB signify that the repeating content is dominant, and ILC should allow the error signal to enter the learning update. Therefore $Q(z)$ should be set to a value of 1 at frequencies where $\mathrm{RNR} > 0$ dB, but should be close to zero at frequencies where $\mathrm{RNR} < 0$ dB. For the $K(z)$ design, frequencies with $\mathrm{RNR} < 0$ dB should be targeted to minimize the dominant non-repeating error. This is done by designing the weighting functions, W_S and W_T, such that the magnitude of $S(z) \ll 0$ dB at these particular frequencies, which indicates that the error is effectively mitigated. The second design component of ILC is the learning function, $L(z)$. From the discussion of plant inversion ILC in Section II-B, we know that any change in the feedback controller causes a change in $L(z)$. Therefore, $L(z)$ should be designed after $K(z)$.

Experimental testing of the system tracking is then required to evaluate the performance of the combined controller design as in step 4 of Fig. 4. If the tracking objectives were not achieved, then an iterative approach is suggested to redesign the combined controller. The error signal obtained after ILC convergence is used in another iteration starting at step 2 whereby a new RNR is determined. This analysis provides valuable insight into how the repeating and non-repeating error content has reduced in comparison to the original signal analysis. Then, feedback and feedforward controllers can be redesigned if necessary. Sections IV-A–IV-D discuss this design approach on several scenarios with different exogenous signal content.

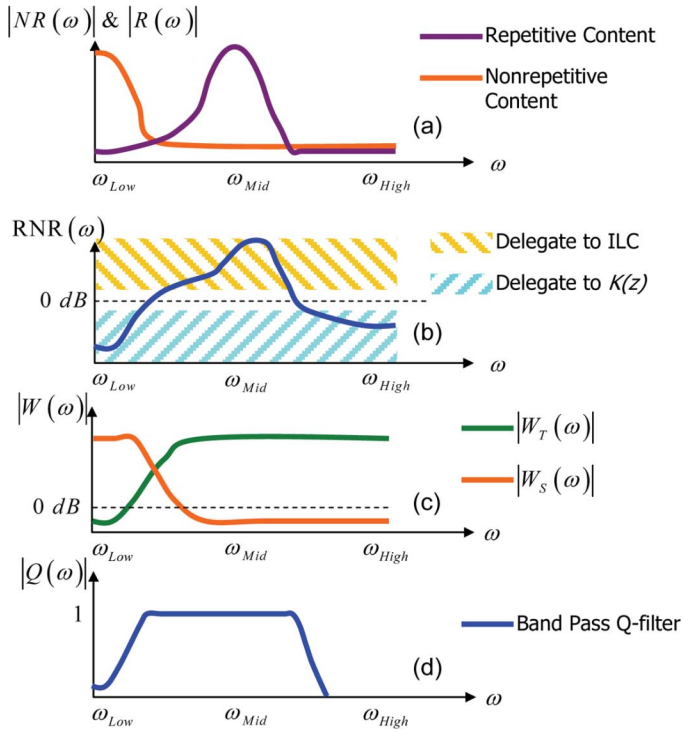

Fig. 5. Scenario #1: (a) $R(\omega)$ and $\mathrm{NR}(\omega)$; (b) RNR; (c) H_∞ weighting functions; and (d) Q-filter.

A. Scenario #1

The first scenario can be seen in Fig. 5(a) and (b). Large non-repeating error content appears at ω_{Low}, and large repeating content exists around ω_{Mid} range. From the RNR plot 5b, we clearly notice that the non-repeating content dominates the repeating content at ω_{Low}, whereas the relationship is switched around ω_{Mid}. ILC will be effective if it learns exclusively at the ω_{Mid} range, so a band pass type of Q-filter will enable this type of learning. The H_∞-feedback controller should be designed to mitigate the dominant non-repeating error at ω_{Low}. Therefore, our combined controller design consists of a H_∞-feedback controller with low frequency error mitigation, and an ILC controller design with a band pass Q-filter. The general shapes of the band pass Q-filter and H_∞ weighting functions are shown in Fig. 5(c) and (d).

B. Scenario #2

The next scenario in Fig. 6 has large non-repeating exogenous signal content at ω_{Low}, but the RNR remains above 0 dB at low and mid frequencies. Due to the RNR having a value greater than 0 dB up to ω_{High}, ILC should be allowed to learn all of the

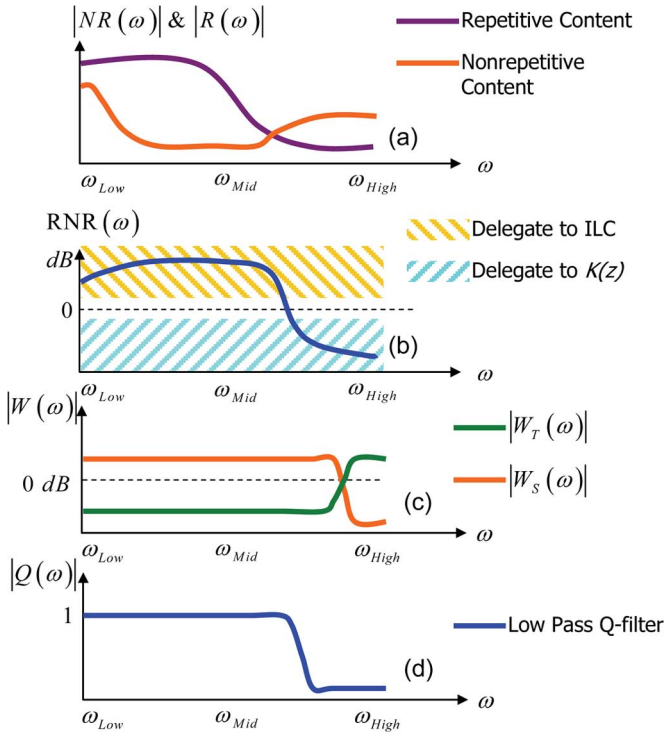

Fig. 6. Scenario #2: (a) $R(\omega)$ and $\mathrm{NR}(\omega)$; (b) RNR; (c) H_∞ weighting functions; and (d) Q-filter.

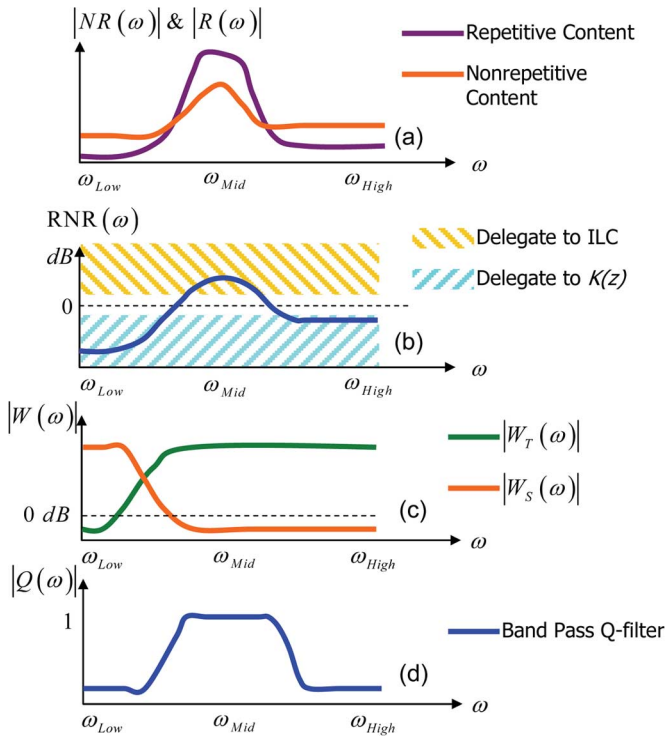

Fig. 7. Scenario #3: (a) $R(\omega)$ and $\mathrm{NR}(\omega)$; (b) RNR; (c) H_∞ weighting functions; and (d) Q-filter.

low to mid-frequency error content. A low pass Q-filter would then be designed for ILC. As for $K(z)$, the non-repeating error dominates between ω_{Mid} and ω_{High} as indicated by the $\mathrm{RNR} < 0$ dB. To minimize these effects, $K(z)$ should be designed to have high bandwidth in attempt to reduce this error. The suggested design uses a low pass Q-filter and a high bandwidth H_∞-feedback controller. This suggested controller design may have inadequate performance, because of the large magnitude of non-repeating error that exists at ω_{Low}, which was not clearly identified by the RNR. Following experimental tests, the error data could be used to iterate on the first design.

C. Scenario #3

The plots for the last scenario in Fig. 7 illustrate an RNR curve that is similar to that of Section IV-A. With this RNR contour, the Q-filter should be a band pass type as discussed previously. The H_∞-feedback controller should be focused on minimizing the error in the frequency band where the $\mathrm{RNR} < 0$ dB, which is in the ω_{Low} region. The combined controller design would be a band pass type Q-filter and a $K(z)$ that reduces low-frequency error content. Again, the combined controller design suggested here may need to be iterated upon due to the existence of non-repeating content near ω_{Mid}. The $K(z)$ design was intended to mitigate error near ω_{Low}, so it would not effectively reduce the large amount of non-repeating content.

D. Scenario Summary

The preceding sections developed several possible scenarios with varying exogenous signal content, and in each scenario a first iteration combining H_∞-feedback and ILC design was suggested. The selection of $K(z)$ is not limited to a H_∞ controller, but this type is investigated throughout this work due to the frequency domain design. In order to make the integration seamless, we advise that $K(z)$ be selected such that its design is done in the frequency domain.

A summary of the suggested controller designs has been produced in Table I. It should be noted that there is a large number of possibilities when it comes to scenarios of exogenous repeating and non-repeating signals. Therefore, the combined controller designs are in no way limited by the summary in the following table. Further discussion is included in [30].

V. Experimental Results

The aforementioned design procedure was implemented on two different nanopositioning systems in order to properly illustrate this approach. These two nanopositioning devices are termed the NanoCube and the parallel kinematic mechanism (PKM). The former is actuated by piezo electric actuators in a serial architecture and is commercially available from Physik Instrumente as model P-611.3S. The PKM is also actuated by piezos, but in a parallel architecture. It was designed at the University of Illinois at Urbana-Champaign, and the interested reader is referred to [31] for a detailed discussion on its kinematics and design. Both systems use a dSPACE DS1104 DSP controller board for data acquisition and control at a sampling rate of 4 kHz.

These devices are considered MIMO systems, since each system has three actuators (inputs) and shows movement in the x, y, and z spatial dimensions (outputs). An approximate range of motion for all of the piezos is 100 μm. For means of illustration and simplicity, this work treats the NanoCube

TABLE I
CONTROLLER DESIGN SUMMARY FOR DIFFERENT SCENARIOS

Four Control Scenarios		ILC Q-filter Design	
		Low Pass	Band Pass
H_∞ Feedback Controller Designs	Low Bandwidth	$RNR(\omega) > 0dB \; \forall \; \omega < \omega_{High}$ Large NR(ω) at ω_{Low}	$RNR(\omega) > 0dB \; \forall \; \omega_{Low} < \omega < \omega_{High}$ Large NR(ω) at ω_{Low}
	High Bandwidth	$RNR(\omega) > 0dB \; \forall \; \omega < \omega_{High}$ Large NR(ω) at ω_{Mid}	$RNR(\omega) > 0dB \; \forall \; \omega_{Low} < \omega < \omega_{High}$ Large NR(ω) at ω_{Mid}

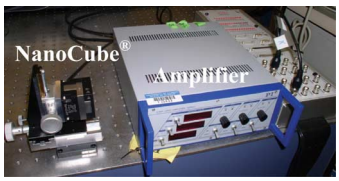

Fig. 8. NanoCube experimental setup.

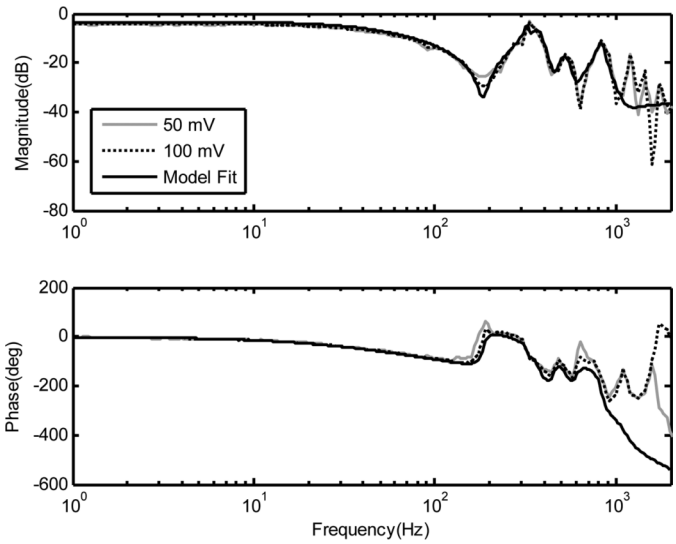

Fig. 9. System identification model fit.

as a SISO system, in which only the x-axis is used for precise positioning control. This was feasible due to the serial and decoupled kinematics of the NanoCube, where only one actuator caused movement in the x-direction. Following the SISO system discussion, we use the parallel actuator structure of the PKM as a testbed for controller design on a MIMO positioning system. The PKM system experiences a different set of exogenous signal content than the NanoCube system that complements the reasoning behind the proposed design procedure. Sections V-A and V-B, which discuss the results from the NanoCube and PKM, respectively.

A. SISO Experimental System

Fig. 8 above shows the Physik Instrumente NanoCube and E-664 Controller (amplifier) system setup. Frequency domain system identification was performed on the x-axis by fitting a model to the frequency response curves seen in Fig. 9. The model fit was a 12th-order discrete LTI model (19). High frequency pole-zero pairs in the model cause model inaccuracy

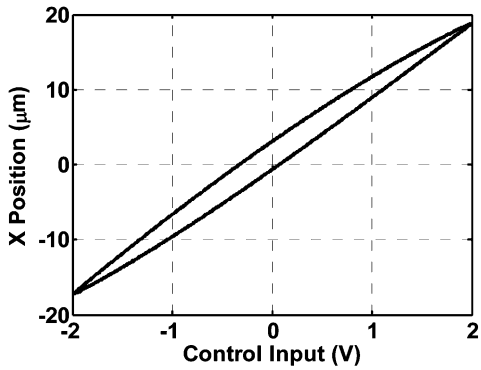

Fig. 10. Hysteresis plot from experimental open-loop response of NanoCube.

above 100 Hz. Therefore, controller designs had bandwidths below 100 Hz

$$G(z) = \frac{\begin{array}{c}0.025031\,(z-0.5323)\left(z^2-1.891z+0.9723\right)\\ \left(z^2-1.703z+0.9595\right)\left(z^2-1.462z+0.9289\right)\\ \left(z^2-1.109z+0.8855\right)\left(z^2-0.4932z+1.719\right)\end{array}}{\begin{array}{c}(z-0.6193)(z-0.9251)\left(z^2-1.294z+0.5162\right)\\ \left(z^2-1.723z+0.9719\right)\left(z^2-1.589z+0.9055\right)\\ \left(z^2-1.268z+0.8754\right)\left(z^2-0.502z+0.8917\right)\end{array}}. \tag{19}$$

As with many piezo actuated systems, the NanoCube shows hysteretic behavior. This nonlinear effect is common with typical voltage driven piezo systems and is difficult to eliminate. Custom-built charge amplifiers [32] can be used to significantly reduce this effect in hardware. Fig. 10 shows the open-loop hysteresis in this system. Nonlinear hysteresis models [32] typically include an internal state variable to capture the direction dependent characteristics. This internal state is dependent on the reset path in which the positioner has taken. If the positioner is not reset to its initial condition in exactly the same trajectory prior to tracking, the internal hysteresis state is altered. This causes the controller to output a different initial control effort from trial to trial in order to hold the positioner at the same initial condition. This change in the controller output is typically a dc offset, which explains why hysteresis is considered a low frequency phenomenon.

The reset command was designed to change the reset path prior to tracking each iteration in effort to induce a non-repeating hysteresis effect. This is typically a problematic scenario for ILC. Normally when ILC is used, all initial conditions and exogenous signals are assumed to be identical every iteration. It should be noted that ILC was not utilized for tracking the non-repeating reset path. The reference, $r(z)$, is shown later in

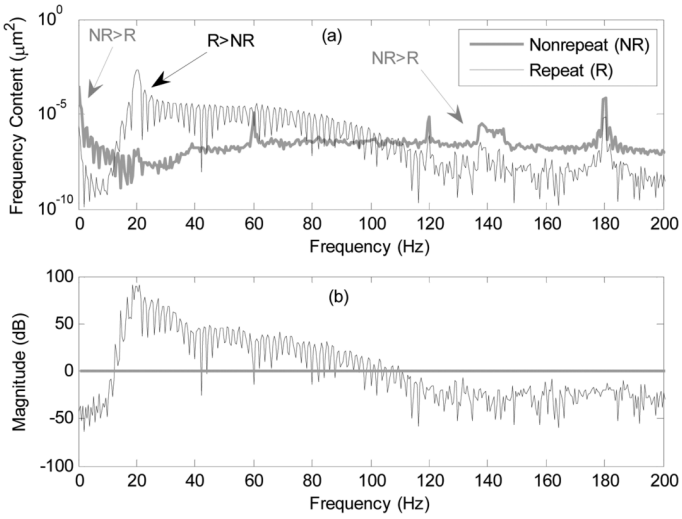

Fig. 11. (a) Error periodogram for repeatable $d(z)$ and nonrepeatable, $d_j(z)$. (b) RNR of signal power.

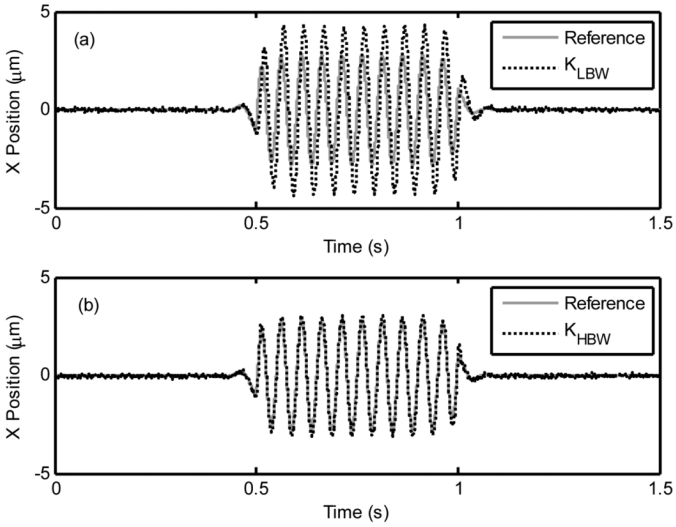

Fig. 13. (a) K_{LBW} and (b) K_{HBW} feedback tracking.

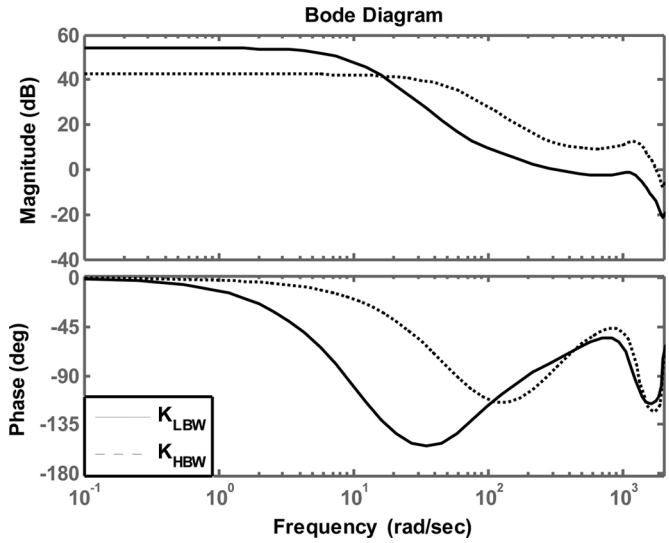

Fig. 12. Bode plot of H_∞ controller designs.

TABLE II
FOUR CONTROLLER SCENARIOS

Four Control Scenarios		ILC Q-filter Design	
		Low Pass	Band Pass
H_∞ Feedback Controller Designs	Low Bandwidth	Reduce low frequency effects	Approach presented here
	High Bandwidth	Typical Design	Approach presented here

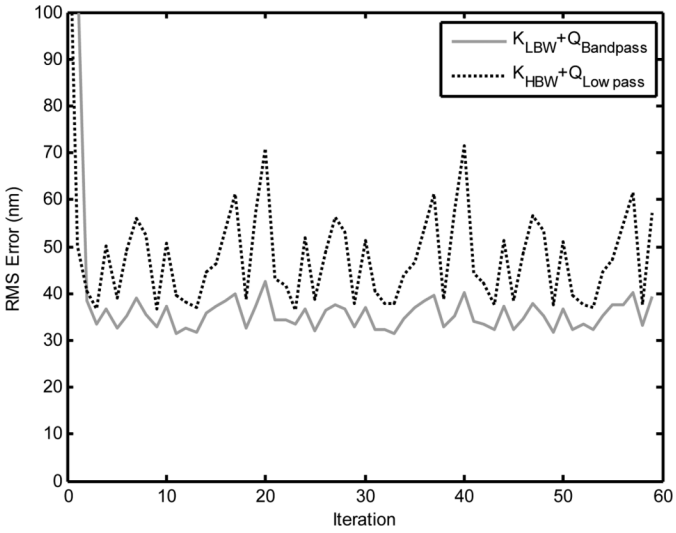

Fig. 14. RMS tracking error versus iteration.

Fig. 13. The dominant signal content occurs at 20 Hz. There is a clear frequency separation, as in Fig. 5(a), between the low frequency non-repeating hysteresis content and the repeating content of $r(z)$.

A stabilizing H_∞-feedback controller was designed to collect reference signal tracking data for signal analysis purposes. Signal analysis produced repeating and non-repeating content periodograms as seen in Fig. 11(a). The large low frequency non-repeating content represents the hysteresis effect in the piezo actuator. From the RNR plot in Fig. 11(b), the repetitive error appears to be dominant in the frequency range between 10–100 Hz. This leads to the design of a Q-filter for ILC that has a value of one for frequencies between 10 and 100 Hz, and a small value for all other frequencies. By definition this Q-filter design is a band pass filter. In the operating frequency range, i.e., 0–100 Hz, the $\mathrm{RNR} < 0$ dB below 15 Hz, which suggests that $K(z)$ be designed to mitigate error in this low frequency region. Thus, the combined design then utilizes a H_∞-feedback controller with low frequency disturbance rejection and a band pass Q-filter.

Due to constraints from (6), there is typically a tradeoff between system bandwidth and low frequency disturbance rejection when designing a robust H_∞-feedback controller. In this

TABLE III
FEEDBACK + ILC STATISTICS

RMS error statistics for four controller scenarios (iter. 3-60)			ILC Q-filter Design	
			Low Pass	Band Pass
Feedback	Low Bandwidth	Mean	35.9 nm	35.4 nm
		Standard Dev.	3.3 nm	2.8 nm
	High Bandwidth	Mean	46.0 nm	41.1 nm
		Standard Dev.	8.0 nm	3.6 nm

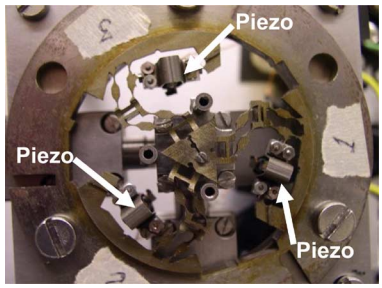

Fig. 15. Top view of PKM.

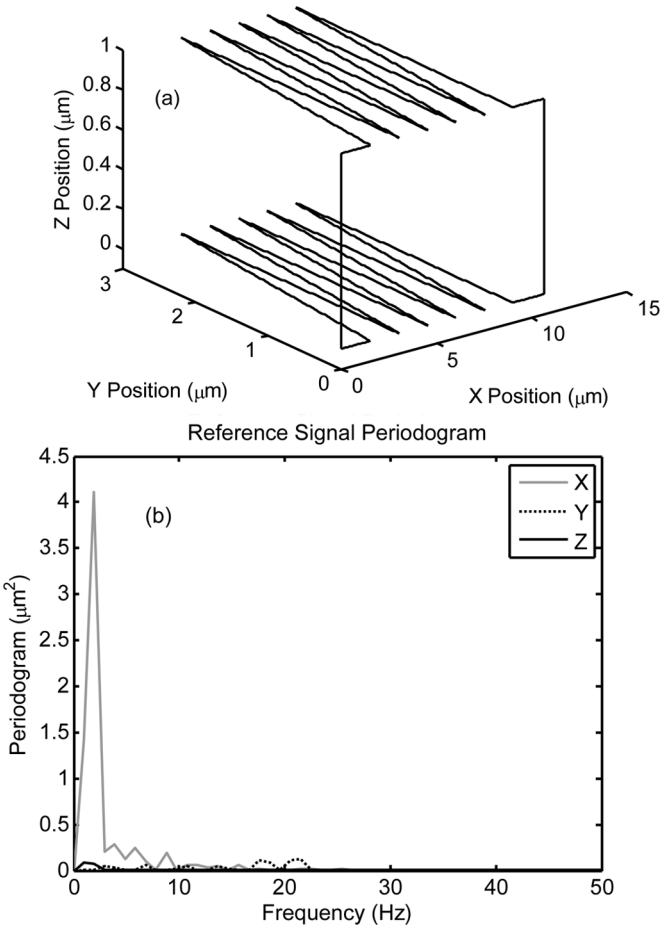

Fig. 16. (a) PKM reference signal. (b) Reference signal periodogram.

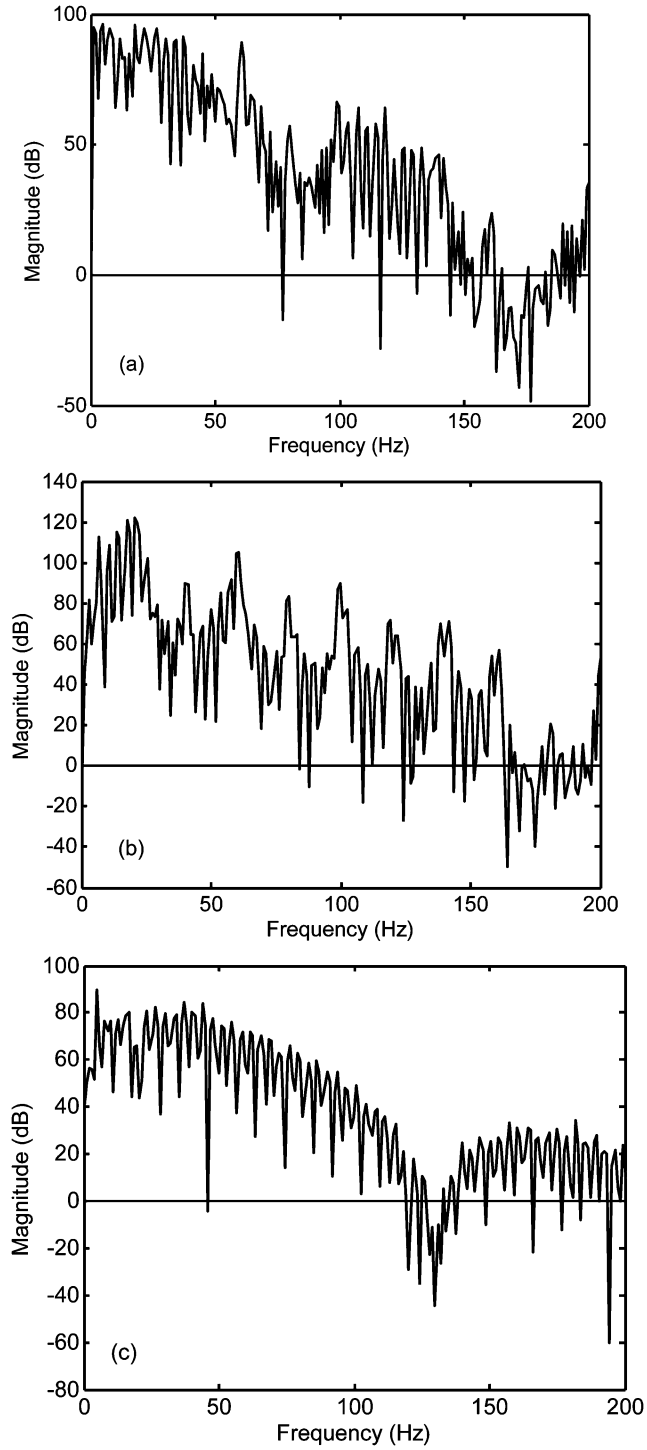

Fig. 17. Initial RNR for: (a) X-axis; (b) Y-axis; (c) Z-axis.

work, we have two $K(z)$ designs, in which this tradeoff is observed. The first design, K_{LBW}, has large gains at low frequency to mitigate low frequency error content as suggested by the RNR, but the closed-loop system bandwidth was only 15 Hz. The other controller, K_{HBW}, was designed as a standalone feedback controller with a bandwidth of 45 Hz. Their frequency responses are plotted in Fig. 12.

For comparison purposes, two ILC Q-filters were designed, which include a 3rd order Butterworth low pass (0–100 Hz) and band pass (10–100 Hz) filter labeled as Q_{Lowpass} and Q_{Bandpass}, respectively. The two $Q(z)$ and $K(z)$ designs are listed in the Appendix A.1. The plant inverse learning

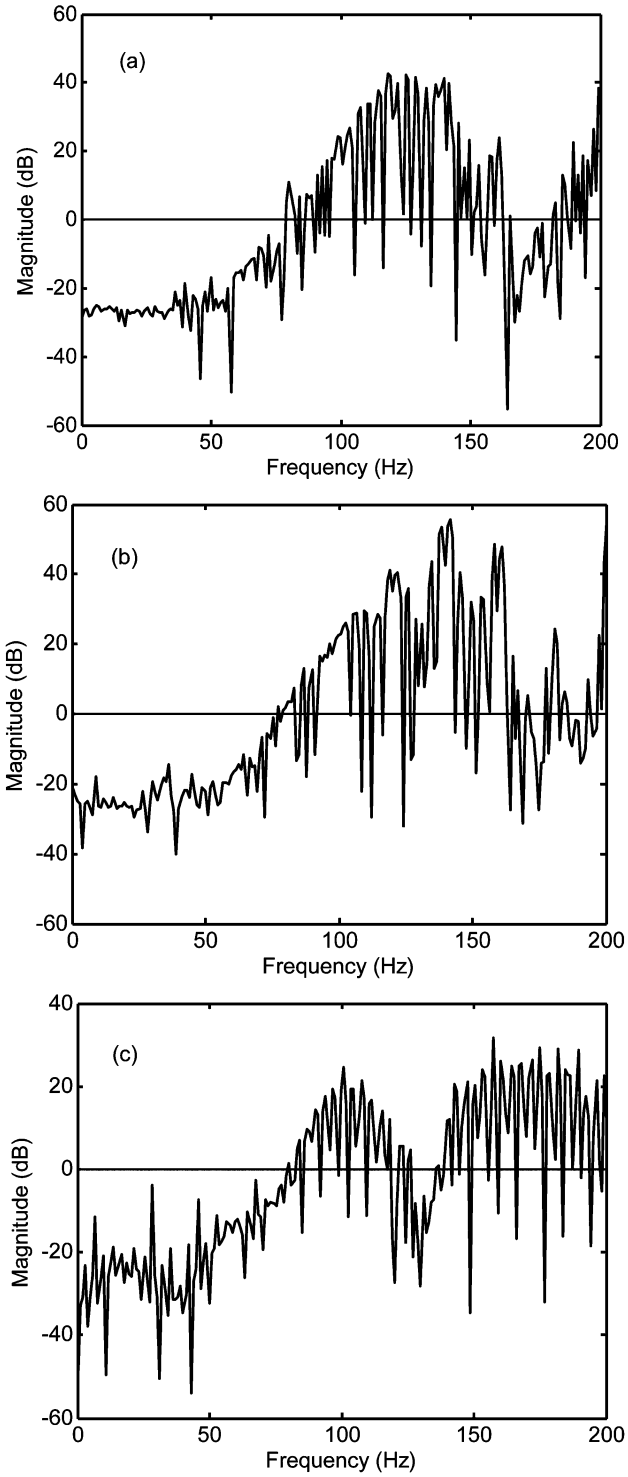

Fig. 18. Second Iteration RNR for: (a) X-axis; (b) Y-axis; (c) Z-axis.

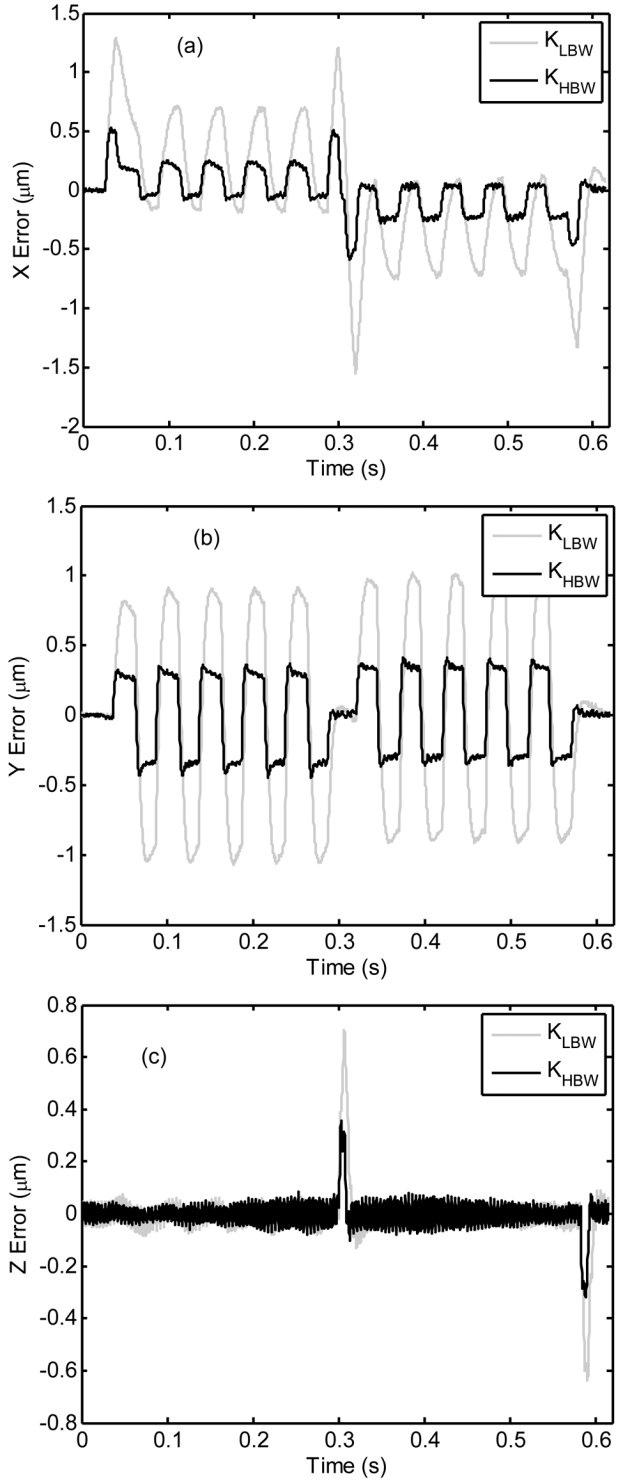

Fig. 19. PKM feedback tracking error for: (a) X-; (b) Y-; and (c) Z-axis.

functions, L_{LBW} and L_{HBW}, for the system with K_{LBW} and K_{HBW} are also shown in the Appendix A.1. A summary of the different controller scenarios is compiled in Table II. The low pass Q-filter and low bandwidth H_∞ control would focus primarily on minimizing the effect of low frequency exogenous signals (references and disturbances) on the system error. The low pass Q-filter and high bandwith H_∞ control is typical of most feedforward/feedback designs in the literature. The right column of Table II indicates novel approaches given here.

To illustrate the difference between the feedback controllers, tracking results are plotted in Fig. 13. The standalone controller, K_{HBW}, clearly tracks the reference with less error than K_{LBW}. This result is expected, because the 20 Hz operating frequency is within the bandwidth of the K_{HBW} system but not of the K_{LBW} system.

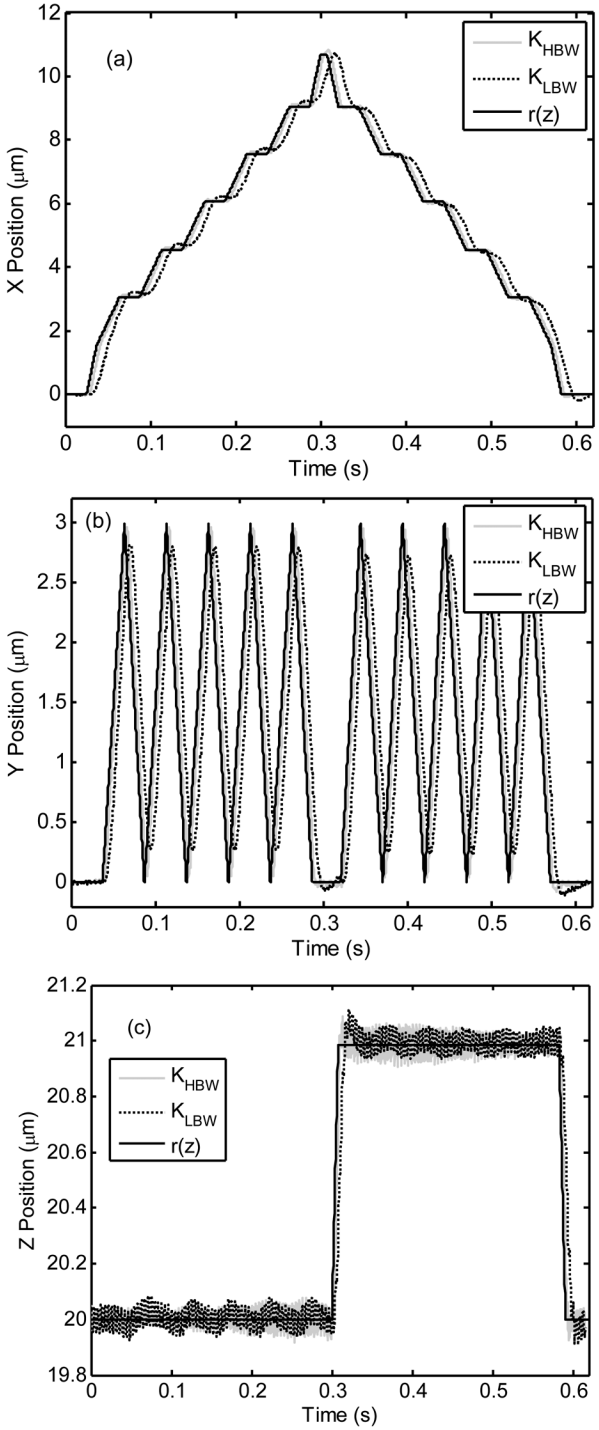

Fig. 20. PKM reference and output signals for: (a) X-; (b) Y-; and (c) Z-axis.

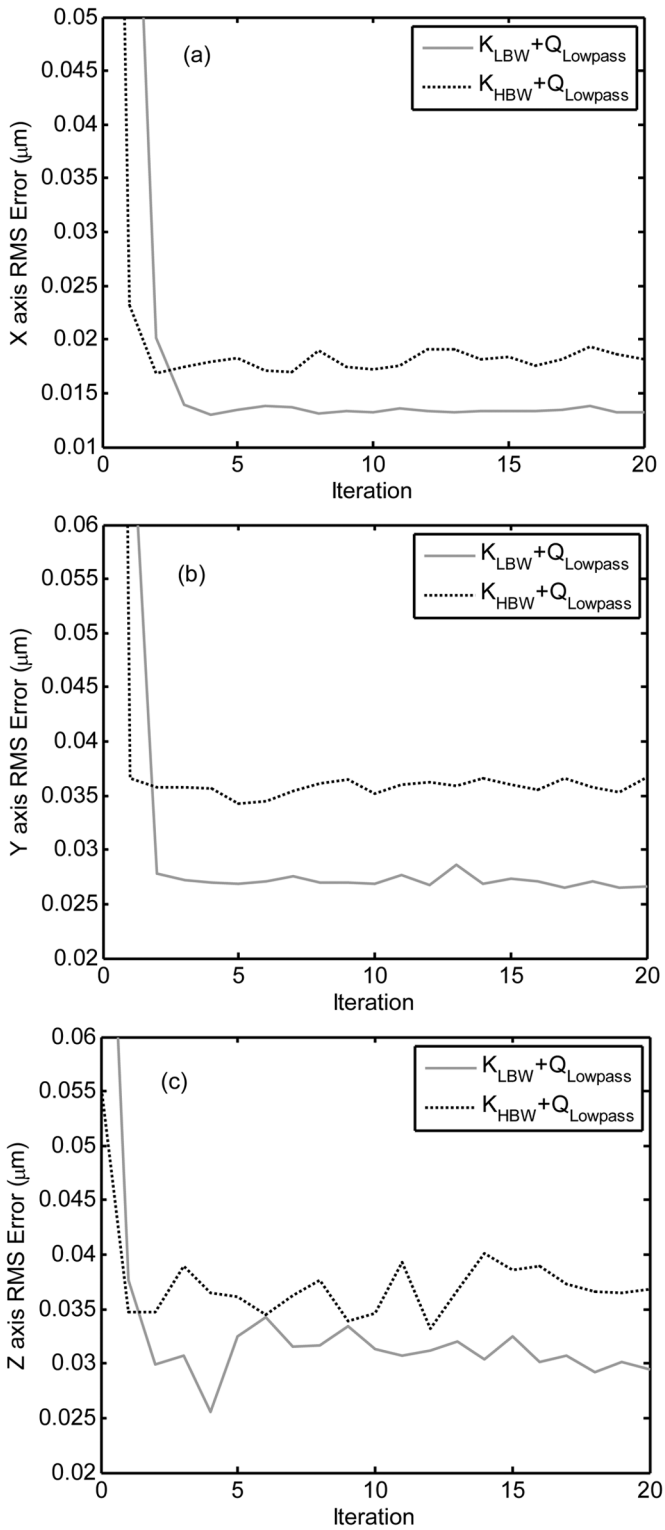

Fig. 21. (a) X-, (b) Y-, and (c) Z-axis RMS error versus iteration.

When ILC is added to the system, the results are less intuitive. First, we introduce the primary performance measure for this work, which is the root mean squared (RMS) error (20). For systems utilizing ILC, this is a common performance metric [10], and it should also be stated that a control system achieving lower RMS error is considered more desirable. When K_{LBW} and K_{HBW} controllers are used with ILC, large decreases in RMS error are recorded after ILC convergence, which occurs by the third iteration. Fig. 14 plots the RMS error per iteration, and the control scenario with the lower RMS error was $K_{\mathrm{LBW}} + Q_{\mathrm{Bandpass}}$. In typical ILC and feedback controller design, a $K_{\mathrm{HBW}} + Q_{\mathrm{Lowpass}}$ type of configuration would be considered the more suitable control scenario, because these two

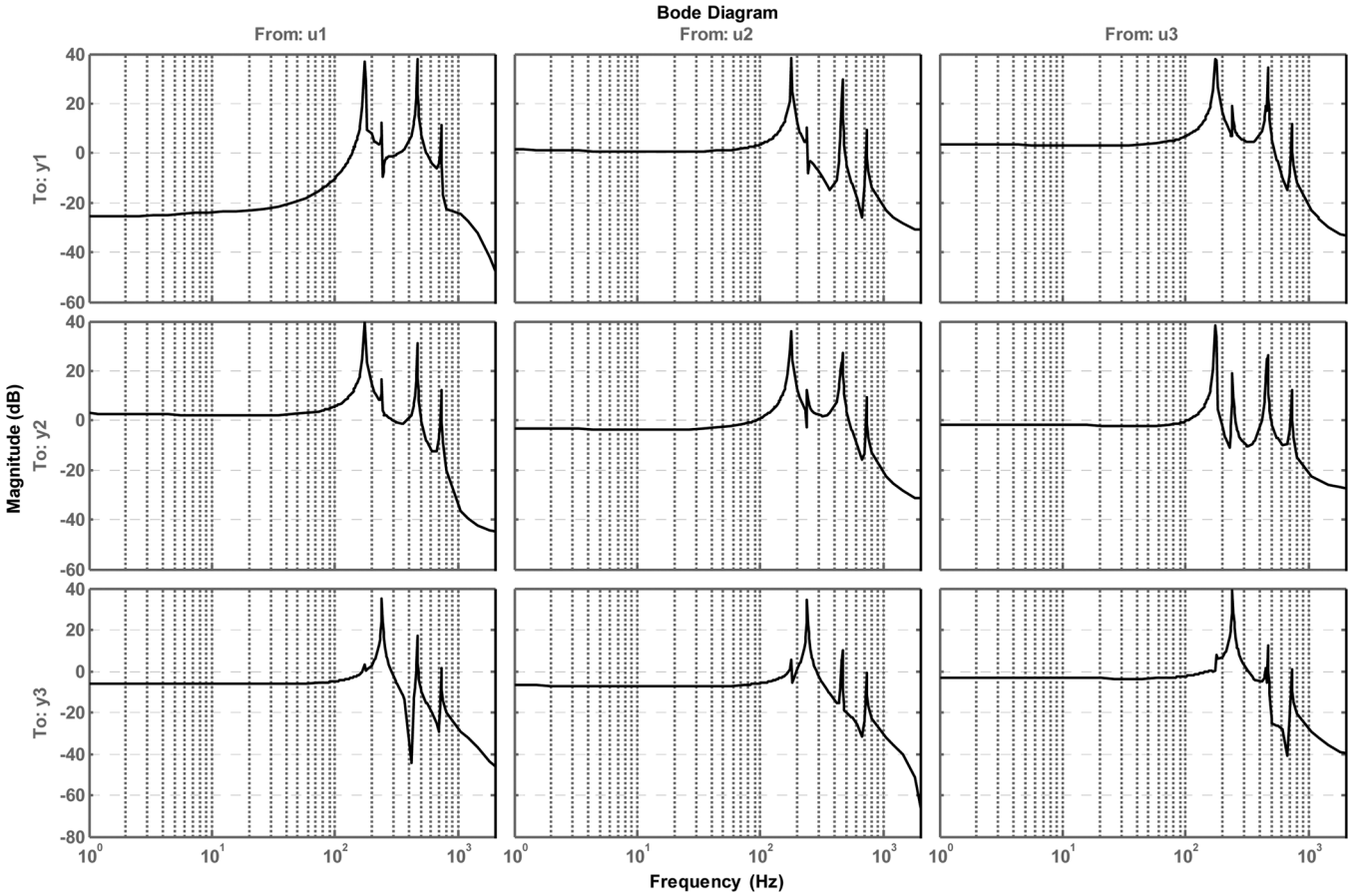

Fig. 22. Bode magnitude diagram of PKM model.

designs are thought of as being superior in their respective control areas. Statistical results from these experimental tests are summarized in Table III

$$e_{\mathrm{RMS}} = \frac{\sqrt{\sum_{i=1}^{N} |e_i|^2}}{\sqrt{N}}. \tag{20}$$

We conclude from the experimental results that signal analysis provides valuable intuition, which leads to the appropriate combined design of feedback and ILC controllers. Better performance was obtained by using an atypical choice for $K(z)$ and $Q(z)$. The low frequency disturbance rejection of K_{LBW} mitigates these effects better than K_{HBW}. This is supported by the results in Table III where K_{LBW} has lower average RMS error than K_{HBW}. The RNR plot was the critical component of this design approach, because this plot identified frequency ranges with dominant repeating or non-repeating error. The results validate this RNR approach by pointing out that Q_{Bandpass} provides better performance than Q_{Lowpass}.

B. MIMO Experimental System

The PKM in Fig. 15 is actuated by the use of three piezo actuators and flexure linkages. Capacitance gages and the A/D of the dSPACE DS1104 were used to measure the position of the PKM with resolution of 2 nm. For the interested reader, additional control results using this testbed were explored in [33] and [34].

Time domain system identification was performed using a PRBS input on each actuator, producing three different responses. A single-input multiple-output (SIMO) discrete LTI model was estimated for each actuator, and then compiled into a final MIMO model. Each SIMO model was estimated by a discrete LTI model with 13 states based on the Hankel Singular Value decomposition. Combining three of these models resulted in a final discrete MIMO LTI model with 39 states. As seen in Fig. 22, the PKM model has large system resonances above 100 Hz, so the operating frequency range of this system will be below 100 Hz, similar to the NanoCube in Section V-A.

A 3-D reference signal was devised in the form of a raster scanning pattern, shown in Fig. 16(a). This tracking pattern had a constant velocity of 125 μm/s, and the scanning frequency was approximately 20 Hz. The individual axes periodograms are plotted in Fig. 16(b), where it can be seen that the majority of signal content lies below 25 Hz. The periodograms did not plot above 200 Hz due to absence of significant error content.

Tracking data was collected for multiple iterations in order to conduct signal analysis, which is discussed here. The RNR plots for the x, y, and z axes are displayed in Fig. 17. These plots show a different scenario than that of the NanoCube in Section V-A. Here, $\mathrm{RNR} > 0$ dB at all frequencies below 100 Hz. This suggests that a low pass Q-filter be designed for the ILC. For the

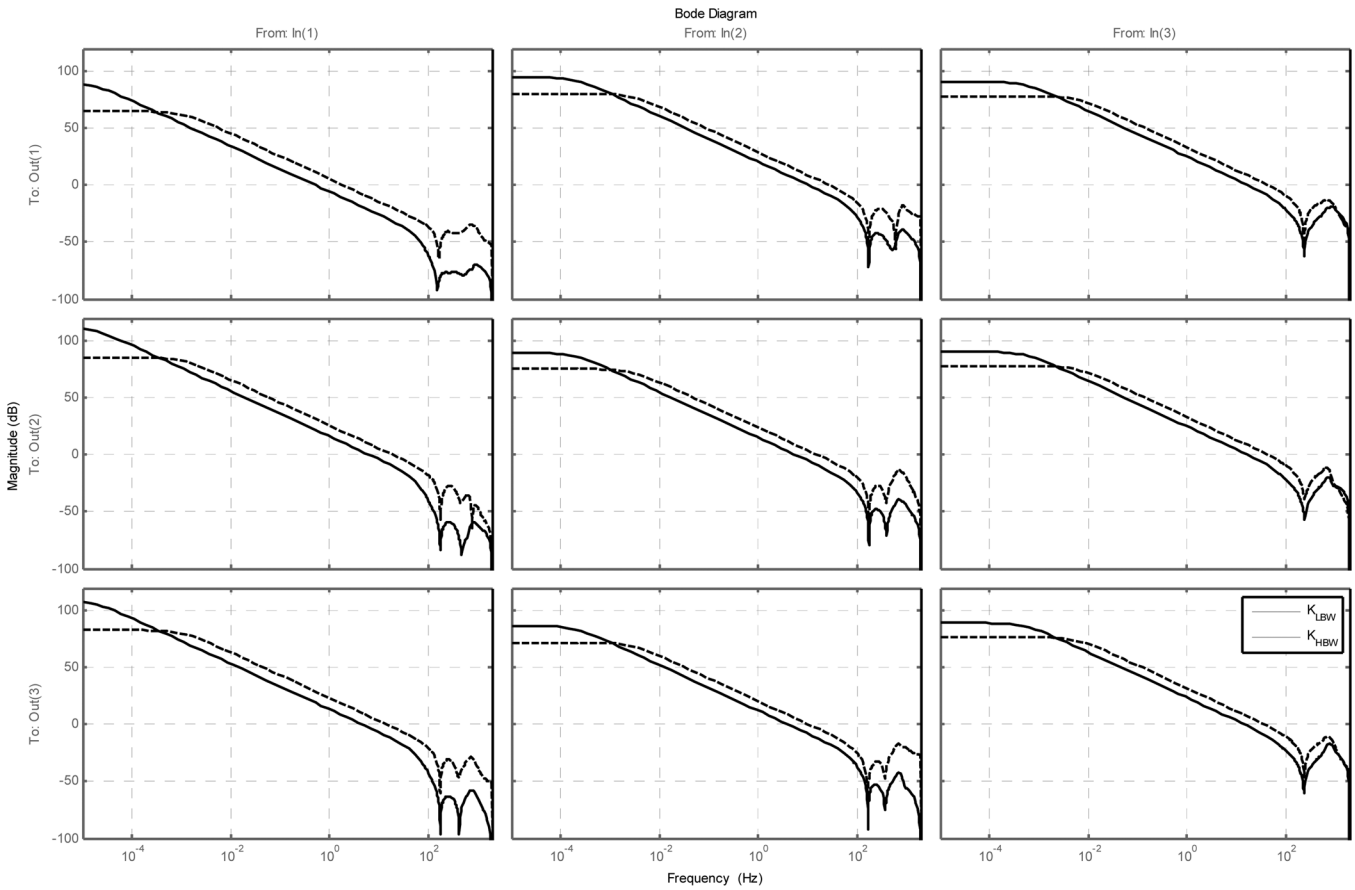

Fig. 23. Bode magnitude diagram of H_∞ controller designs.

H_∞-feedback controller design, it is not clear as to what frequency range should be delegated to $K(z)$, because in the operating range the $\mathrm{RNR} > 0$ dB. Thus, we disregard the signal analysis, and design a potential stand-alone $K(z)$. The Bode magnitude diagrams for the low pass $Q(z)$ and the standalone $K(z)$ designs can be found in Figs. 23 and 24, respectively.

Before presenting results from the combined controller, we need to design different $Q(z)$ and $K(z)$ functions to compare performance. The new combined controllers were developed using the iterative method in steps 5–7 of Fig. 4. Signal analysis was performed on tracking data obtained from testing the first controller design, and the RNR plots are shown in Fig. 18.

The plots in Fig. 18 show that the low pass $Q(z)$ has allowed ILC to eliminate the repeating error dominance at frequencies below 50 Hz, because the $\mathrm{RNR} < 0$ dB. The alternative $K(z)$ design should then mitigate the low frequency non-repeating error. In doing so, the tradeoff for low frequency error mitigation is a lower system bandwidth. This $K(z)$ design had x-, y-, and z-axes bandwidths of 10, 15, and 20 Hz due to constraints on the size of the controller. We will refer to this controller as K_{LBW}, because all axes have a lower bandwidth than the 30, 40, and 50 Hz bandwidths of the x-, y-, and z-axes of the first $K(z)$ design, which is labeled K_{HBW}. The performance of the K_{HBW} controller is very similar to that given in [33], [34] since the design weightings were very similar. Therefore, K_{HBW} can be thought of as the best feedback controller developed to date for this PKM system.

For comparison purposes, an additional $Q(z)$ design was produced, which was a band pass type filter (1–100 Hz). This alternate $Q(z)$ design is named Q_{Bandpass}, whereas the initial Q-filter is referred to as Q_{Lowpass}. Frequency response plots for the $K(z)$ and $Q(z)$ designs can be seen in Appendix B.2. The two $Q(z)$ discrete LTI functions can be found in [30] along with the two $K(z)$ and $L(z)$ functions used to produce these experimental results.

Comparing the tracking results of K_{LBW} and K_{HBW} without ILC in Figs. 19 and 20, it is apparent that K_{HBW} has significantly less tracking error than K_{LBW}. This is an expected result. However, when ILC is added to the positioning system, the results are not as intuitive. Fig. 21 shows the converged RMS error reduction when using $K_{\mathrm{LBW}} + Q_{\mathrm{Lowpass}}$ or, the more typical, $K_{\mathrm{HBW}} + Q_{\mathrm{Lowpass}}$ design. Again, we observe that the atypical design, $K_{\mathrm{LBW}} + Q_{\mathrm{Lowpass}}$, has lower converged RMS error in the x, y, and z directions. Results with Q_{Bandpass} were poor due to the high RNR value in Fig. 17 for all frequencies up to 100 Hz, so these results were not plotted. From Fig. 19, it should be noted that the RMS values for the feedback controllers without feedforward were on the order of 0.2 μm for the K_{HBW} case and 0.5–1.0 μm for the K_{LBW} case. Therefore, the use of feedforward lowered the RMS tracking error by approximately an order of magnitude. Statistics for all $\mathrm{feedforward}+\mathrm{feedback}$ controller scenarios can be viewed in Appendix B.1.

In the piezo actuated PMC systems of this section, we expect to see significant quantities of non-repeating content at very

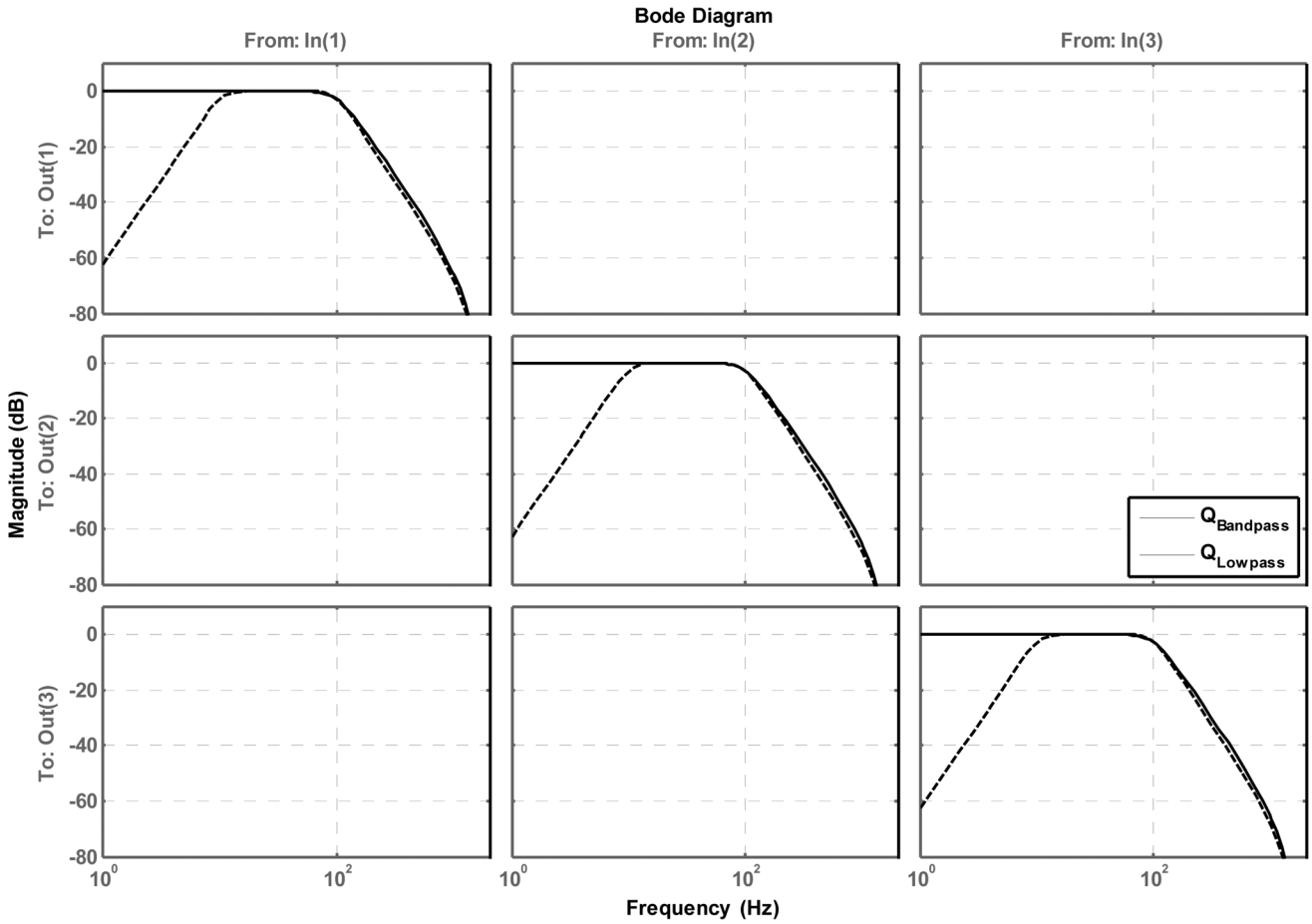

Fig. 24. Bode magnitude diagram of Q-filter designs.

low frequencies due to the nonlinear hysteresis in the piezos. Both examples in this work used piezo actuators and showed this effect. The goal of the feedback controller design was relatively similar in both systems, in that the $K(z)$ was designed to minimize the low frequency error within the system. However, the Q-filter design in these examples provided different results due to the ratio of repeating to non-repeating content occurring at low frequencies, or as introduced here, the RNR. This design approach is applicable to different types of PMC systems utilizing ILC, not just piezo actuated PMC systems.

VI. Conclusion

The combined controller design process presented in this paper introduces a novel approach for frequency domain delegation between feedback and feedforward controller authority; specifically H_∞ and ILC. The design approach incorporates the identification of different classes of error signals, i.e., repeatable and nonrepeatable, through a novel function: the RNR ratio. The RNR ratio determines the frequency range in which feedback or feedforward control should be employed. Through a combined controller design approach, appropriate frequency domain weighting functions for H_∞-feedback and Q-filters have been discussed and proven to be effective from experimental results of two PMC systems. This design process is an improvement upon typical ILC, where the feedback controller design is decoupled from that of the ILC design.

TABLE IV
Error Statistics for PKM Tests

RMS error stats (iterations 2-20)				ILC Q-filter Design	
				$Q_{Lowpass}$	$Q_{Bandpass}$
X-Axis	Feedback	K_{LBW}	Mean	17.6 nm	356 nm
			Std. Dev.	16.6 nm	2.0 nm
		K_{HBW}	Mean	18.3 nm	124 nm
			Std. Dev.	1.4 nm	0.4 nm
Y-Axis	Feedback	K_{LBW}	Mean	29.6 nm	116 nm
			Std. Dev.	10.8 nm	6.0 nm
		K_{HBW}	Mean	35.8 nm	61.6 nm
			Std. Dev.	0.6 nm	0.6 nm
Z-Axis	Feedback	K_{LBW}	Mean	31.3 nm	48.5 nm
			Std. Dev.	2.4 nm	1.4 nm
		K_{HBW}	Mean	36.6 nm	36.0 nm
			Std. Dev.	2.0 nm	1.4 nm

Appendix A

Nanocube Transfer Functions: See equations (A.1)–(A.6) at the top of the next page.

Appendix B

PKM Performance Statistics: See Table IV.
PKM Frequency Response Plots: See Figs. 22–24.

$$L_{\mathrm{LBW}}(z)=\frac{\begin{array}{l}17.067(z+0.9435)(z-0.925)(z-0.5294)\left(z^2-1.914z+0.916\right)\left(z^2-1.964z+0.965\right)\left(z^2-0.7285z+0.8636\right)\\ \left(z^2-0.857z+0.2483\right)\left(z^2-1.782z+0.8648\right)\left(z^2-1.293z+0.5156\right)\left(z^2-1.716z+0.9615\right)\\ \left(z^2-1.723z+0.9727\right)\left(z^2-1.587z+0.9042\right)\left(z^2-1.482z+0.8835\right)\left(z^2-1.269z+0.848\right)\left(z^2-1.272z+0.8817\right)\end{array}}{\begin{array}{l}z(z-0.5293)(z-0.5318)(z-0.8987)(z+0.9436)(z-0.9969)^3\left(z^2-1.11z+0.8759\right)\left(z^2-0.7288z+0.8641\right)\\ \left(z^2-0.8514z+0.2412\right)\left(z^2-1.788z+0.8715\right)\left(z^2-1.89z+0.9716\right)\left(z^2-1.716z+0.9621\right)\\ \left(z^2-1.703z+0.9595\right)\left(z^2-1.479z+0.8829\right)\left(z^2-1.461z+0.9264\right)\left(z^2-1.27z+0.8531\right)\end{array}} \tag{A.1}$$

$$L_{\mathrm{HBW}}(z)=\frac{\begin{array}{l}17.067(z+0.9465)(z-0.9249)(z-0.6161)\left(z^2-1.761z+0.7758\right)\left(z^2-1.874z+0.883\right)\left(z^2-1.261z+0.8895\right)\\ \left(z^2-0.2907z+0.06567\right)\left(z^2-1.729z+0.8289\right)\left(z^2-1.285z+0.5099\right)\left(z^2-1.715z+0.9585\right)\\ \left(z^2-1.724z+0.9755\right)\left(z^2-1.581z+0.9004\right)\left(z^2-1.49z+0.907\right)\left(z^2-1.223z+0.8352\right)\left(z^2-0.5869z+0.7496\right)\end{array}}{\begin{array}{l}z(z-0.5311)(z-0.6699)(z-0.9837)^3(z+0.9466)\left(z^2-0.2614z+0.0582\right)\left(z^2-1.89z+0.9716\right)\\ \left(z^2-1.787z+0.8849\right)\left(z^2-1.716z+0.9619\right)\left(z^2-1.703z+0.9595\right)\left(z^2-1.483z+0.9068\right)\\ \left(z^2-1.461z+0.9264\right)\left(z^2-1.214z+0.8528\right)\left(z^2-1.11z+0.8759\right)\left(z^2-0.5959z+0.7582\right)\end{array}} \tag{A.2}$$

$$Q_{\mathrm{Lowpass}}(z)=\frac{0.00041655(z+1)^3}{(z-0.8541)(z^2-1.832z+0.8549)} \tag{A.3}$$

$$Q_{\mathrm{Bandpass}}(z)=\frac{0.00030812(z-1)^3(z+1)^3}{\begin{array}{l}(z-0.9798)\left(z^2-1.986z+0.9863\right)\\ (z-0.8856)\left(z^2-1.859z+0.8804\right)\end{array}} \tag{A.4}$$

$$K_{\mathrm{HBW}}(z)=\frac{\begin{array}{l}0.56966(z+1)(z+0.8803)(z-0.925)(z-0.6135)(z-0.2905)^2\left(z^2-0.7768z+0.9227\right)\\ \left(z^2-1.902z+0.9055\right)\left(z^2-1.309z+0.5305\right)\left(z^2-1.734z+0.9736\right)\left(z^2-1.611z+0.9125\right)\left(z^2-1.338z+0.8926\right)\end{array}}{\begin{array}{l}(z+0.9466)\left(z^2-1.787z+0.8849\right)(z-0.9837)^3\left(z^2-0.2614z+0.05821\right)\left(z^2-1.214z+0.8528\right)\\ \left(z^2-1.716z+0.9619\right)(z-0.5286)\left(z^2-1.483z+0.9068\right)\left(z^2-0.5959z+0.7852\right)(z-0.6699)\end{array}} \tag{A.5}$$

$$K_{\mathrm{LBW}}(z)=\frac{\begin{array}{l}0.12369(z+1)(z+0.5941)(z-0.6718)^2(z-0.6135)(z-0.925)\left(z^2-1.974z+0.9744\right)\left(z^2-0.7768z+0.9227\right)\\ \left(z^2-1.309z+0.5305\right)\left(z^2-1.734z+0.9736\right)\left(z^2-1.611z+0.9125\right)\left(z^2-1.338z+0.8926\right)\end{array}}{\begin{array}{l}(z+0.9436)(z-0.8987)(z-0.9969)^3(z-0.5293)\left(z^2-0.8514z+0.2412\right)\left(z^2-1.788z+0.8715\right)\left(z^2-1.338z+0.8926\right)\\ \left(z^2-1.716z+0.9621\right)\left(z^2-1.479z+0.8829\right)\left(z^2-1.27z+0.8531\right)\left(z^2-0.7288z+0.8641\right)\left(z^2-1.611z+0.9125\right)\end{array}}. \tag{A.6}$$

ACKNOWLEDGMENT

The authors would like to thank Dr. J. Lewis for the use of the NanoCube.

REFERENCES

[1] S. Devasia, E. Eleftheriou, and S. Moheimani, "A survey of control issues in nanopositioning," *IEEE Trans. Control Syst. Technol.*, vol. 15, no. 5, pp. 802–823, Sep. 2007.

[2] D. Bristow and A. Alleyne, "A high precision motion control system with application to microscale robotic deposition," *IEEE Trans. Control Syst. Technol.*, vol. 14, no. 6, pp. 1008–1020, Nov. 2006.

[3] S. Skogestad and I. Postlethwaite, *Multivariable Feedback Control: Analysis and Design*. New York: Wiley, 2005.

[4] J. C. Doyle, B. A. Francis, and A. Tannenbaum, *Feedback Control Theory*. Toronto, ON, Canada: Maxwell Macmillan International, 1992.

[5] Y. Okazaki, "A micro-positioning tool post using a piezoelectric actuator for diamond turning machines," *Precision Eng.*, vol. 12, pp. 151–156, Jul. 1990.

[6] R. C. Barrett and C. F. Quate, "Optical scan-correction system applied to atomic force microscopy," *Rev. Scientific Instruments*, vol. 62, pp. 1393–1399, Jun. 1991.

[7] S. Arimoto, S. Kawamura, and F. Miyazaki, "Bettering operation of robots by learning," *J. Robot. Syst.*, vol. 1, pp. 123–140, 1984.

[8] K. L. Moore, *Iterative Learning Control for Deterministic Systems*. New York: Springer-Verlag, 1993.

[9] Z. Bien and J. Xu, *Iterative Learning Control: Analysis, Design, Integration and Applications*. Norwell, MA: Kluwer, 1998.

[10] D. Bristow, M. Tharayil, and A. Alleyne, "A survey of iterative learning control," *IEEE Control Syst. Mag.*, vol. 26, pp. 96–114, 2006.

[11] A. Sebastian and S. Salapaka, "Design methodologies for robust nanopositioning," *IEEE Trans. Control Syst. Technol.*, vol. 13, no. 6, pp. 868–876, Nov. 2005.

[12] B. Dijkstra, "Iterative learning control with applications to a waferstage," Ph.D. dissertation, Mech. Eng. Dept., TU Eindhoven, Eindhoven, The Netherlands, 2004.

[13] G. Heinzinger, D. Fenwick, B. Paden, and F. Miyazaki, "Stability of learning control with disturbances and uncertain initial condition," *IEEE Trans. Autom. Control*, vol. 37, no. 1, pp. 110–114, Jan. 1992.

[14] S. S. Saab, "On the P-type learning control," *IEEE Trans. Autom. Control*, vol. 39, no. 11, pp. 2298–2302, Nov. 1994.

[15] Y. Chen, C. Wen, Z. Gong, and M. Sun, "An iterative learning controller with initial state learning," *IEEE Trans. Autom. Control*, vol. 44, no. 2, pp. 371–376, Feb. 1999.

[16] C. J. Chien, C. T. Hsu, and C. Y. Yao, "Fuzzy system-based adaptive iterative learning control for nonlinear plants with initial state errors," *IEEE Trans. Fuzzy Syst.*, vol. 12, no. 5, pp. 724–732, Oct. 2004.

[17] S. Salapaka, A. Sebastian, J. P. Cleveland, and M. V. Salapaka, "High bandwidth nano-positioner: A robust control approach," *Rev. Scientific Instruments*, vol. 73, pp. 3232–3241, 2002.

[18] H. Kwakernaak, "Robust control and H infinity-optimization—tutorial paper," *Automatica*, vol. 29, pp. 255–273, 1993.

[19] H. W. Bode, *Network Analysis and Feedback Amplifier Design*. New York: D. Van Nostrand Company, Inc., 1946.

[20] J. S. Freudenberg and D. P. Looze, "Right half plane poles and zeros and design tradeoffs in feedback systems," *IEEE Trans. Autom. Control*, vol. 30, no. 6, pp. 555–565, Jun. 1985.

[21] B. Wu and E. Jonckheere, "A simplified approach to Bode's theorem for continuous-time and discrete-time systems," *IEEE Trans. Autom. Control*, vol. 37, no. 11, pp. 1797–802, Nov. 1992.

[22] G. Balas, R. Chiang, A. Packard, and M. Safanov, *Robust Control Toolbox 3*. Natick, MA: The Mathworks, Inc.

[23] T. Sogo, "Stable inversion for nonminimum phase sampled-data systems and its relation with the continuous-time counterpart," in *Proc. 41st IEEE Conf. Dec. Control*, Las Vegas, NV, Dec. 2002, pp. 3730–3735.

[24] Q. Zou and S. Devasia, "Preview-based stable-inversion for output tracking of nonlinear nonminimum-phase systems: The VTOL example," *Automatica*, vol. 43, no. 1, pp. 117–127, 2007.

[25] D. A. Bristow, "Frequency domain analysis and design of iterative learning control for systems with stochastic disturbances," presented at the Amer. Control Conf., Seattle, WA, Jun. 2008.

[26] T. Kavli, "Frequency domain synthesis of trajectory learning controllers for robot manipulators," *J. Robot. Syst.*, vol. 9, pp. 663–680, 1992.

[27] B. E. Helfrich, C. Lee, D. A. Bristow, X. H. Xiao, J. Dong, A. G. Alleyne, S. M. Salapaka, and P. M. Ferreira, "Combined H_∞-feedback and iterative learning control design with application to nanopositioning systems," in *Proc. Amer. Control Conf.*, Seattle, WA, Jun. 2008, pp. 3893–3900.

[28] L. Ljung, *System Identification: Theory for the User*. Englewood Cliffs, NJ: Prentice-Hall PTR, 1999.

[29] L. Ljung, *System Identification Toolbox 7*. Natick, MA: The Mathworks, Inc.

[30] B. E. Helfrich, "Coordinated design of H_∞-feedback and iterative learning control with application to nanopositioning systems," M.S. thesis, Mech. Eng. Dept., Univ. Illinois, Urbana, 2008.

[31] Q. Yao, J. Dong, and P. M. Ferreira, "A novel parallel-kinematics mechanisms for integrated, multi-axis nanopositioning: Part 1. Kinematics and design for fabrication," *Precision Eng.*, vol. 32, pp. 7–19, Jan. 2008.
[32] M. Goldfarb and N. Celanovic, "Modeling piezoelectric stack actuators for control of micromanipulation," *IEEE Control Syst. Mag.*, vol. 17, no. 3, pp. 69–79, Jun. 1997.
[33] J. Dong, Q. Yao, and P. M. Ferreira, "A novel parallel-kinematics mechanism for integrated, multi-axis nanopositioning: Part 2: Dynamics, control and performance analysis," *Precision Eng.*, vol. 32, pp. 20–33, Jan. 2008.
[34] J. Dong, S. M. Salapaka, and P. M. Ferreira, "Robust control of a parallel kinematic nano-positioner," *ASME J. Dyn. Syst., Meas., Control*, vol. 130, no. 4, 2008, 041007.

Brian E. Helfrich received the B.S. degree from Purdue University, West Lafayette, IN, in 2006 and the M.S. degree from the University of Illinois at Urbana-Champaign, Urbana-Champaign, in 2008, both in mechanical engineering.

He is currently a Systems Engineer with Sandia National Laboratories, Albuquerque, NM. While working towards the B.S. degree, he completed the cooperative education program with Toyota Motor Manufacturing Indiana as a Manufacturing Engineer, and during his pursuit of the M.S. degree, he was a Research Assistant with the Center for Nanoscale Chemical-Electrical-Mechanical Manufacturing Systems (Nano-CEMMS). His research focused on precision motion control utilizing combined efforts from H-infinity feedback control and iterative learning control.

Chibum Lee (S'08) was born in Seoul, Korea, in 1975. He received the B.S. and M.S degrees in mechanical design and production engineering from Seoul National University, Seoul, Korea, in 1998 and 2000, respectively. He is currently pursuing the Ph.D. degree in mechanical science and engineering, University of Illinois, Urbana-Champaign.

From 2000 to 2005, he was with Hyundai Mobis, Korea as a Dynamics and Control Engineer. His research is primarily focused on the application of control theory to nanoscale systems. He has worked on the development of control design for nanopositioing systems and the new mode for atomic force microscopes.

Douglas A. Bristow received the B.S. degree in mechanical engineering from the Missouri University of Science and Technology, Rolla, in 2001, and the M.S. and Ph.D. degrees in mechanical engineering from the University of Illinois at Urbana-Champaign, Urbana-Champaign, in 2003 and 2007, respectively.

From 2007 to 2008, he was a Postdoctoral Researcher with the Nano-CEMMS at the University of Illinois. In 2008, he joined the Department of Mechanical and Aerospace Engineering, Missouri University of Science and Technology, where he is an Assistant Professor. His research interests include precision motion control and nanopositioning systems.

X. H. Xiao received the B.S. and M.S. degrees in mechanical engineering from Wuhan University, Wuhan, China, in 1991 and 1998, respectively, and the Ph.D. degree in mechanical engineering from the Huazhong University of Science and Technology, Wuhan, China, in 2005.

She joined Wuhan University in 1998, where she is currently an Associate Professor with the Mechanical Engineering Department, School of Power and Mechanical Engineering. She has published over 30 papers in the areas of mobile robots, dynamics and control, sensors and signal procession. From 2006 to 2008, she worked as a visiting Professor with the University of Illinois at Urbana-Champaign. Her current research interests include high-precision positioning control, mobile robotics, and signal processing.

Jingyan Dong received the B.S. degree in automatic control from the University of Science and Technology of China, Hefei, China, in 1998, the M.S. degree from the Institute of Automation, Chinese Academy of Sciences, Beijing, China, in 2001, and the Ph.D. degree in mechanical engineering from the University of Illinois at Urbana-Champaign, Urbana-Champaign, in 2006.

From 2006 to 2008, he was a Postdoctoral Research Associate with the Center for Nanoscale Chemical-Electrical-Mechanical Manufacturing Systems (Nano-CEMMS), the University of Illinois at Urbana-Champaign. Since 2008, he has been a faculty member with the Department of Industrial and Systems Engineering, North Carolina State University, Raleigh. His research interests include micro/nano manufacturing, multidimensional scale mechatronics and manufacturing systems, and their design, fabrication, sensing, control and application to micro/nano/macro manipulation and manufacturing.

A. G. Alleyne received the B.S.E. degree in mechanical and aerospace engineering from Princeton University, Princeton, NJ, in 1989 and the M.S. and Ph.D. degrees in mechanical engineering from The University of California at Berkeley, Berkeley, in 1992 and 1994, respectively.

He joined the University of Illinois, Urbana-Champaign, in 1994, where he currently holds the Ralph M. and Catherine V. Fisher Professorship in the College of Engineering. He was a Fulbright Fellow to the Netherlands where he held a Visiting Professorship in Vehicle Mechatronics at TU Delft. His research interests include a mix of theory and implementation with a broad application focus.

Dr. Alleyne was a recipient of the ASME Dynamics Systems and Control Division's Outstanding Young Investigator Award and the 2008 ASME Gustus L. Larson Memorial Award. He is a Fellow of the ASME.

Srinivasa M. Salapaka (M'93) was born in Andhra Pradesh, India, in 1973. He received the B.Tech. degree in mechanical engineering from the Indian Institute of Technology, Chennai, India, in 1995 and the M.S. and Ph.D. degrees in mechanical engineering from the University of California, Santa Barbara, in 1997 and 2002, respectively.

From 2002 to 2004, he was a Postdoctoral Associate with the Laboratory for Information and Decision Systems, Massachusetts Institute of Technology, Cambridge. Since 2004, he has been a Faculty Member in mechanical science and engineering, University of Illinois, Urbana-Champaign. His current research interests include controls for nanotechnology, combinatorial resource allocation, and numerical analysis of integral equations.

Dr. Salapaka was a recipient of the National Science Foundation CAREER Award in 2005.

Placid M. Ferreira received the Ph.D. degree in industrial engineering from Purdue University, West Lafayette, IN, in 1987.

Currently, he is the Grayce Wicall Gauthier Professor of Mechancial Science and Engineering at the University of Illinois at Urbana-Champaign, Urbana-Champaign, where he directs the NSF-sponsored Center for Nanoscale Chemical-Electrical-Mechanical Manufacturing Systems (Nano-CEMMS). His research interests include precision engineering, automation and control of manufacturing systems, MEMS and nanoscale manufacturing.